EARLY QUARK DECONFINEMENT IN COMPACT STAR ASTROPHYSICS AND HEAVY-ION COLLISIONS*

O. Ivanytskyi, D. Blaschke, T. Fischer

Institute of Theoretical Physics, University of Wroclaw, Poland

A. Bauswein

GSI Helmholtzzentrum für Schwerionenforschung, Darmstadt, Germany

Received 16 August 2022, accepted 14 October 2022, published online 14 December 2022

Based on a recently developed relativistic density functional approach to color-superconducting quark matter and a novel quark–hadron transition construction which phenomenologically accounts for the effects of inhomogeneous pasta phases and quark–hadron duality, we construct a class of hybrid equations of state applicable at the regimes typical for compact star astrophysics and heavy-ion collisions. We outline that early quark deconfinement is a notable consequence of strong diquark pairing providing a good agreement with the observational data and driving the trajectories of the matter evolution during the supernova explosions toward the regimes typical for the compact star mergers and heavy-ion collisions.

DOI:10.5506/APhysPolBSupp.16.1-A104

1. Introduction

The puzzling question of the origin of compact stars (CS) with masses exceeding $2M_\odot$ can be successfully addressed at present only within the supernova (SN) explosion mechanism based on quark deconfinement in the stellar matter [1]. This serves as an indirect argument in favor of the existence of quark matter in cores of heavy CS. Binary CS mergers could produce a distinct postmerger gravitational wave signal [2]. These interesting applications are summarised in [3]. They are based on a hybrid equation of state (EoS) that has been constructed from hadronic and quark matter EoS developed within relativistic density functional (RDF) approaches. In this contribution, we summarize recent developments of the RDF approach to quark matter which address beyond confinement also the aspects of chiral

* Presented at the 29th International Conference on Ultrarelativistic Nucleus–Nucleus Collisions: Quark Matter 2022, Kraków, Poland, 4–10 April, 2022.

symmetry breaking and color superconductivity. In particular, the occurrence of a large diquark pairing gap modifies the phase structure and EoS of QCD at low temperatures, and is thus of central interest for the discussion of the existence and location of one or more critical endpoints (CEPs). A developed constructive scheme generates thermodynamically consistent EoS with multiple or absent CEPs and provides a solid basis for discussing their effects in simulations of astrophysical phenomena and heavy-ion collisions (HIC).

2. Relativistic density functional for quark matter

The RDF approach from Ref. [4] is represented by the Lagrangian

$$\mathcal{L} = \bar{q}(i\partial\!\!\!/ - m)q - G_{\rm V}(\bar{q}\gamma_\mu q)^2 + G_{\rm D}(\bar{q}i\gamma_5\tau_2\lambda_A q^c)(\bar{q}^c i\gamma_5\tau_2\lambda_A q) - \mathcal{U} \quad (1)$$

with two-flavor quark field $q^T = (u\ d)$, current quark mass m, and $G_{\rm V}$, $G_{\rm D}$ being coupling constants in vector repulsion and diquark pairing channels, respectively. A chirally symmetric generalization of the potential energy density functional inspired by the string-flip model (SFM) [5] reads

$$\begin{aligned}\mathcal{U} &= D_0\left[(1+\alpha)\langle\bar{q}q\rangle_0^2 - (\bar{q}q)^2 - (\bar{q}i\gamma_5\vec{\tau}q)^2\right]^{\frac{1}{3}} \\ &\simeq \mathcal{U}_{\rm MF} + (\bar{q}q - \langle\bar{q}q\rangle)\Sigma_{\rm MF} - G_{\rm S}\left(\bar{q}q - \langle\bar{q}q\rangle\right)^2 - G_{\rm PS}\left(\bar{q}i\gamma_5\vec{\tau}q\right)^2 . \quad (2)\end{aligned}$$

Here, α and D_0 are constants and $\langle\bar{q}q\rangle_0$ is the chiral condensate in the vacuum. The last line in Eq. (2) corresponds to the second-order expansion of $\mathcal{U}$ around the mean-filed solutions $\langle\bar{q}q\rangle$ and $\langle\bar{q}i\gamma_5\vec{\tau}q\rangle = 0$ labeled with the subscript index MF. This expansion brings the present model to the form of the NJL model with the mean-field scalar self-energy of quarks $\Sigma_{\rm MF} = \partial\mathcal{U}_{\rm MF}/\partial\langle\bar{q}q\rangle$ and effective couplings in scalar $G_{\rm S} = -\partial\mathcal{U}^2_{\rm MF}/\partial\langle\bar{q}q\rangle^2/2$ and pseudoscalar $G_{\rm PS} = -\partial\mathcal{U}^2_{\rm MF}/\partial\langle\bar{q}i\gamma_5\vec{\tau}q\rangle^2/6$ channels. In Ref. [4], model parameters $m = 4.2$ MeV, $\Lambda = 573$ MeV, $\alpha = 1.43$, and $D_0\Lambda^{-2} = 1.39$ were fixed in order to reproduce the pion mass $M_\pi = 140$ MeV and decay constant $F_\pi = 92$ MeV, with the scalar meson mass $M_\sigma = 980$ MeV and the vacuum value of the chiral condensate per flavor $\langle\bar{l}l\rangle_0 = -(267\ \text{MeV})^3$. We note that Λ is a three-momentum scale which occurs in the smooth momentum cut-off by a Gaussian form factor which regularizes divergent zero-point terms. The behavior of $G_{\rm S}$ and $G_{\rm PS}$ as well as the effective quark mass $m^* = m + \Sigma_{\rm MF}$ is shown in Fig. 1. The dynamical breaking of chiral symmetry leads to $G_{\rm S} \neq G_{\rm PS}$ in the vacuum, while its dynamical restoration at high temperatures and/or densities is manifested by the asymptotic coincidence of the scalar and pseudoscalar couplings. This is reflected in the melt-down of m^*. Its vacuum value m_0^* is controlled by the parameter α so that, $m_0^* \to \infty$ at $\alpha \to 0$. For the mentioned set of parameters, $m_0^* = 718$ MeV and the

pseudocritical temperature at $\mu_B = 0$ defined by the peak of the chiral susceptibility is $T_\chi = 163$ MeV. The quark matter EoS is obtained by treating the present model within the mean-field approximation. It is remarkable that the BCS relation between the mass gap in the vacuum and the critical temperature for its restoration, which holds for the (P)NJL model in the chiral limit, is violated for this class of quark matter models.

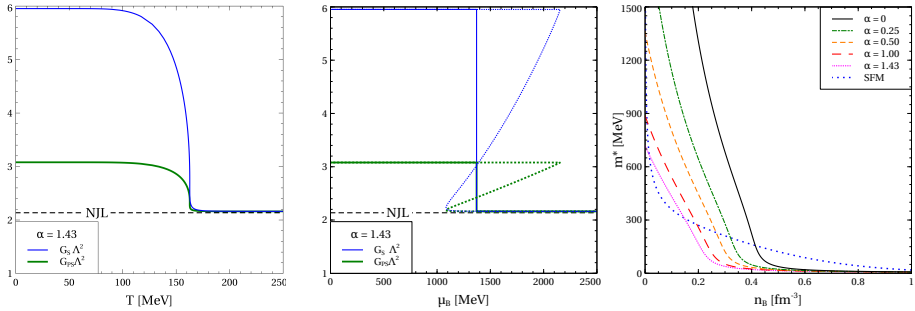

Fig. 1. (Color online) Scaled effective scalar $G_S\Lambda^2$ and pseudoscalar $G_{PS}\Lambda^2$ couplings as functions of temperature T at $\mu_B = 0$ (left panel), baryonic chemical potential μ_B at $T = 0$ (middle panel), and effective quark mass m^* as functions of baryon density n_B (right panel). Dashed lines in the left and right panels represent the NJL value $G\Lambda^2 = 2.14$ from Ref. [6]. Dotted curves in the middle panel indicate the unstable parts that are removed by applying the Maxwell construction. The blue/black sparsely dotted line in the right panel is obtained within the SFM with $\alpha_{\rm SFM} = 0.39$ fm^{-3} [5]. Calculations are performed for symmetric quark matter, $G_V = G_D = 0$, α specified in the legend and the rest of the model parameters with the values mentioned above.

3. Phase diagram of strongly interacting matter

High values of the effective quark mass at low T and μ_B represent phenomenological confinement in the RDF approach. This makes description of strongly interacting matter in terms of quark degrees of freedom inadequate in the confinement region and requires matching the quark matter EoS to the hadron one yielding a hybrid quark–hadron EoS. Within the Maxwell construction of quark–hadron transition, the matching point is defined by the baryon chemical potential $\mu_B^{\rm max}$ at which the pressures of two phases coincide, while the baryon density discontinuously jumps from $n_B^h|_{\rm max}$ on the hadron side to $n_B^q|_{\rm max}$ on the quark one. This picture ignores inhomogeneous structures in the quark–hadron interface known as pasta phases [7] and corresponds to a sharp interface between two phases. Accounting for those, pasta phases would wash out the sharp quark–hadron interface allowing for the existence of a mixed phase, which is restricted by the baryon

chemical potentials μ_B^h and μ_B^q (corresponding to n_B^h and n_B^q) from the hadron and quark sides, respectively. In Ref. [8], the EoS of the pasta phase was parameterized by two pieces of parabolic functions. In Ref. [9], such a two-zone interpolation scheme (TZIS) was further developed to the case of arbitrary fractions of electric charge and applied at finite temperatures. The parameters of these two parabolic functions were defined so that both the pressure p and the baryon density n_B remain continuous at the mixed phase boundaries. Continuity of p is also required at the matching point of two parabolas $\mu_B^c = (\mu_b^h + \mu_B^q)/2$, while n_B experiences a discontinuous jump of Δn_B. The TZIS is given a closed form with the parameterization

$$\mu_B^h = \mu_B^{\max}|_{T=0}(1-x)\sqrt{1-T^2/T_0^2}\,, \qquad \mu_B^q = \mu_B^{\max}(1+x)\,, \tag{3}$$

$$\Delta n_B = n^* \left(T_{\rm cep1} - T\right)^\beta \left(T - T_{\rm cep2}\right)^\beta \theta\left(T_{\rm cep1} - T\right)\theta\left(T - T_{\rm cep2}\right)\,, \tag{4}$$

where $x = 0.01$, $n^* = 0$ or 0.15 fm^{-3}, $T_{\rm cep1} = 90$ MeV and $T_{\rm cep2} = 15$ MeV correspond to high- and low-temperature CEPs, and $\beta = 0.3265$ is the critical exponent of the 3D Ising model universality class [10]. The TZIS allows us to construct a hybrid quark–hadron EoS at arbitrary entropy per baryon s/n_B. Figure 2 compares such an EoS to the one obtained within the Maxwell construction. Furthermore, having the edges of the mixed quark–hadron phase defined, we can construct the phase diagram of strongly interacting matter that is shown in Fig. 3. It is remarkable that the transition from quark to hadron matter leads to a growth of T along adiabates $s/n_B = $ const. being a direct consequence of the reduction of the number of accessible microstates due to the transition to the color superconducting phase of quark matter [4].

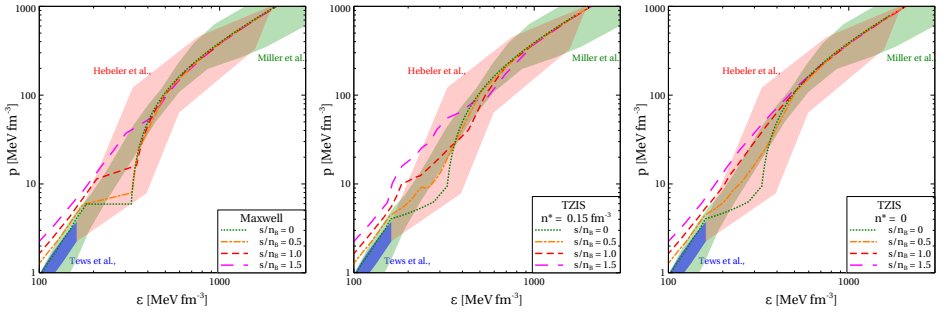

Fig. 2. Pressure p of electrically neutral β-equilibrated quark–hadron matter *vs.* energy density ε along the isentrops $s/n_B = $ const. found within the Maxwell construction (left panel), and the TZIS with $n^* = 0.15$ fm^{-3} (middle panel), and $n^* = 0$ (right panel). The shaded areas represent the cold nuclear matter constraints.

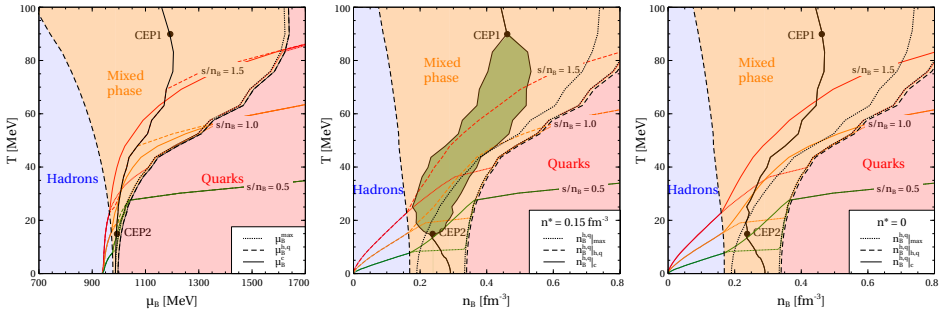

Fig. 3. (Color online) Phase diagram of β-equilibrated electrically neutral quark–hadron matter in the μ_B–T (left panel) and n_B–T (central and right panels) planes. The black dotted, dashed, and solid curves correspond to the phase boundaries and the matching chemical potential discussed in the text. The color mapping of phases corresponds to the TZIS. The filled black circles show the CEPs, which in the right panel are to guide the eye. The colored solid, dashed, and dotted curves show adiabates s/n_B = const. calculated within the Maxwell construction, the TZIS with $n^* = 0.15$ fm^{-3} and $n^* = 0$, respectively. The green/dark gray shaded area in the middle panel shows the region, where n_B discontinuously jumps within the TZIS with $n^* = 0.15$ fm^{-3}.

4. Compact stars at vanishing and finite entropy

Entropy of the quark–hadron matter in the interiors of the proto NS remains approximately constant during SN explosions [1]. Therefore, isentropic EoS of quark–hadron matter is phenomenologically interesting. We applied such EoSs shown in Fig. 2 to solving a problem of relativistic hydrostatic equilibrium [9]. The corresponding mass–radius relations of cold NS ($s/n_B = 0$) and warm proto NS ($s/n_B \neq 0$) are shown in Fig. 4. In the case of cold NS, our approach provides agreement with the constraints

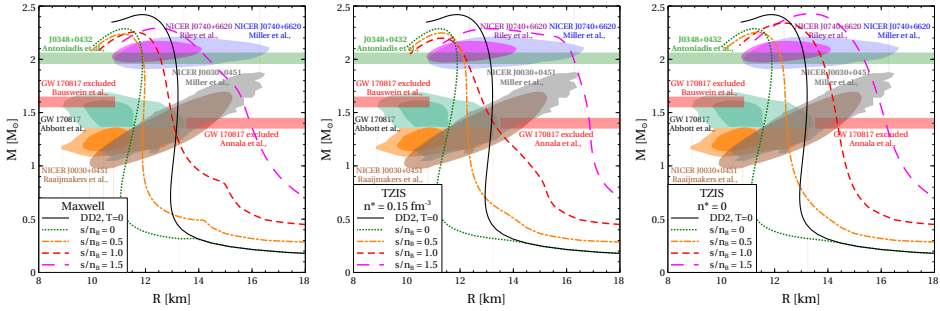

Fig. 4. Mass–radius relation of hybrid NS with the isentropic quark–hadron EoS presented in Fig. 2. Black solid curves obtained with the DD2 EoS of cold hadron matter are given for the sake of comparison. The astrophysical constraints depicted by the colored bands and shaded areas correspond to the case of cold neutron stars.

from Refs. [11–16] and gives the tidal polarizability of $1.4M_\odot$ mass stars $\Lambda_{1.4} = 540$–550 agreeing with Ref. [14]. Finite s/n_B increases the radius of NS but leaves their maximal mass almost unchanged.

5. Conclusions

We developed a confining RDF for color-superconducting quark matter and produced a family of hybrid quark–hadron EoS with or without (multiple) CEPs. Due to the large values of the diquark pairing gap, our approach favors early quark deconfinement, provides good agreement with the present astrophysical constraints, and drives trajectories of the evolution of stellar matter during SN explosions toward the temperatures range of HIC.

This work was supported by the National Science Centre, Poland (NCN) under grants 2019/33/B/ST9/03059 (O.I., D.B.) and 2020/37/B/ST9/00691 (T.F.). A.B. acknowledges support by the European Research Council under the European Union's Horizon 2020 research and innovation program, grant No. 759253, by DFG Project-ID 279384907–SFB 1245, by DFG — Project-ID 138713538–SFB 881 and by the State of Hesse within the Cluster Project ELEMENTS. The work was performed within a project that has received funding from the Horizon 2020 program under grant agreement STRONG-2020 — No. 824093.

REFERENCES

[1] T. Fischer *et al.*, *Nature Astron.* **2**, 980 (2018).
[2] A. Bauswein *et al.*, *Phys. Rev. Lett.* **122**, 061102 (2019).
[3] D. Blaschke, T. Fischer, A. Bauswein, in: C.A.Z. Vasconcellos, F. Weber (Eds.) «Astrophysics in the XXI Century with Compact Stars», *World Scientific*, Singapore 2022.
[4] O. Ivanytskyi *et al.*, *Phys. Rev. D* **105**, 114042 (2022).
[5] M.A.R. Kaltenborn *et al.*, *Phys. Rev. D* **96**, 056024 (2017).
[6] C. Ratti *et al.*, *Phys. Rev. D* **73**, 014019 (2006).
[7] K. Maslov *et al.*, *Phys. Rev. C* **100**, 025802 (2019).
[8] A. Ayriyan *et al.*, *Phys. Rev. C* **97**, 045802 (2018).
[9] O. Ivanytskyi *et al.*, *Eur. Phys. J. A* **58**, 152 (2022).
[10] M. Campostrini *et al.*, *Phys. Rev. E* **65**, 066127 (2002).
[11] T.E. Riley *et al.*, *Astrophys. J. Lett.* **918**, L27 (2021).
[12] M.C. Miller *et al.*, *Astrophys. J. Lett.* **918**, L28 (2021).
[13] T.E. Riley *et al.*, *Astrophys. J. Lett.* **887**, L21 (2019).
[14] B.P. Abbott *et al.*, *Phys. Rev. Lett.* **121**, 161101 (2018).
[15] A. Bauswein *et al.*, *Astrophys. J. Lett.* **850**, L34 (2017).
[16] E. Annala *et al.*, *Phys. Rev. Lett.* **120**, 172703 (2018).